IOP Publishing | International Atomic Energy Agency Nuclear Fusion
Nucl. Fusion **54** (2014) 064010 (7pp) doi:10.1088/0029-5515/54/6/064010

Onset of shearless magnetic surfaces in tokamaks

C. Vieira Abud and I.L. Caldas

Institute of Physics, University of São Paulo, São Paulo, Brazil

E-mail: cabud@if.usp.br

Received 25 June 2013, revised 18 October 2013
Accepted for publication 23 October 2013
Published 23 May 2014

Abstract

The existence of primary shearless tori is a distinguishing feature of nontwist maps. However, secondary shearless tori have been identified in the phase space of twist maps, in the neighbourhood of peculiar bifurcations of elliptic fixed points. In this paper, we report secondary shearless bifurcations in a twist symplectic map that describes chaotic field lines in tokamaks with an ergodic limiter. We identify the onset of secondary shearless tori, around elliptic fixed points within the island of stability, by examining numerical profiles of the internal rotation number. We present examples of field line transport barriers, associated with secondary shearless tori and their rupture, which reduce the usual magnetic field line escape at the tokamak plasma edge.

(Some figures may appear in colour only in the online journal)

1. Introduction

Over the last few years, investigations have indicated that plasma confinement in tokamaks can be controlled by appropriate modifications on the magnetic field at the plasma edge [1]. This control has been achieved by applying resonant perturbations at the plasma edge to alter the magnetic field profile reducing the anomalous particle transport. Most of these perturbations create chaotic field lines in the plasma edge. The presence of chaotic magnetic field lines within the tokamak implies the loss of the plasma confined in this region, due to the destruction of magnetic flux surfaces. Even so, adequate chaotization of field lines at the plasma edge has been found to play a key role in the control of plasma–wall interaction [2–4]. Several tokamaks have been equipped with external devices to induce chaotic field lines, for example, an ergodic limiter [4–7] and a dynamic ergodic divertor [8]. Moreover, currents in external coils have also been applied to create chaos and, consequently, control plasma edge-localized modes [3].

Another favourable situation to improve plasma confinement is the creation of a barrier to reduce field line escape in tokamaks with a reversed magnetic shear profile. Such a barrier is created by means of a nonpeaked plasma current density, corresponding to a nonmonotonic radial profile for the equilibrium safety factor [9]. A resonant magnetic perturbation in the shearless region gives rise to a barrier separating the internal region with magnetic surfaces from the external chaotic region. The presence of the barrier in the shearless region limits the volume of the escape region. All this may contribute to the enhanced plasma confinement, which has been observed in some experiments with magnetic shearless equilibria [10, 11].

As is well known, magnetic field lines can be represented by a 1 + 1/2 degree of freedom Hamiltonian system [12, 13]. Moreover, several properties of these field line Hamiltonian systems can be investigated in associated bidimensional symplectic maps [13, 14]. The advances of symplectic models describing specific features of tokamaks equipped with different devices are remarkable [15]. These maps are introduced to increase the computational capability of investigations on the transport and perform statistical analysis of the chaotic field lines caused by magnetic perturbations. In this framework, the magnetic surfaces are seen as Kolmogorov–Arnold–Moser (KAM) tori and the regular islands along with chaotic lines complete the phase space. In general, Hamiltonian systems or symplectic maps can be classified as twist, for which the rotation numbers increase monotonically; otherwise they are nontwist. The twist condition is assumed in several mathematical theorems such as the Poincaré–Birkhoff theorem, Aubry–Matter theorem and the well-known KAM theorem, which pointed out the persistence of quasi-periodic motion under small perturbations. These theorems are the basis of the twist map scenario but their predictions are not verified for the nontwist maps [13, 14].

Nonetheless, from a topological point of view, the phase spaces of twist and nontwist maps have some remarkable differences. In particular, some peculiar phenomena such as the presence of a nontwist invariant torus and the separatrix reconnection process are only observed in nontwist maps [16–19]. Nevertheless, in [20] the authors studied the resonant normal form around the neighbourhood of elliptic fixed points of symplectic maps and showed that shearless tori (twistless tori) can emerge in twist maps through an atypical bifurcation.

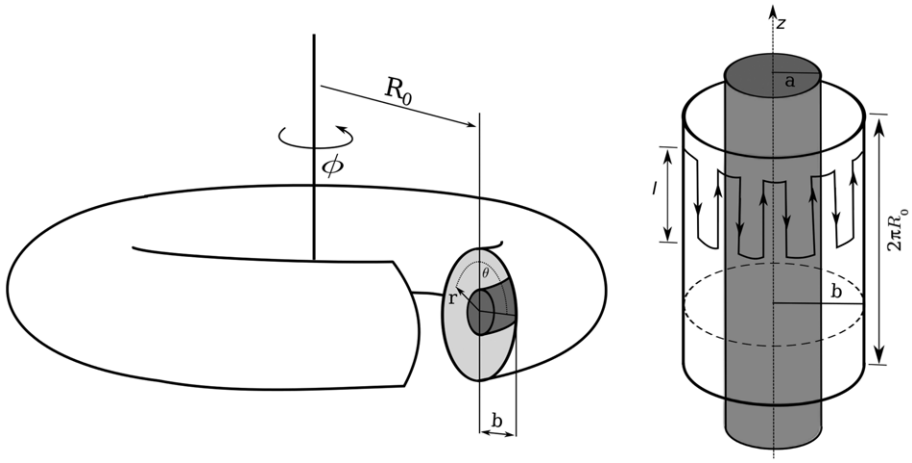

Figure 1. Tokamak scheme showing the main coordinate systems (left) and the $2\pi R_0$-periodic cylindrical approximation (right) where l is the length of the wires of the EML.

Recently, we introduced a numerical procedure to identify shearless tori around elliptic fixed points in twist and nontwist maps. Our procedure was applied to the nontwist and twist standard maps and is based on the variation of the rotation number profile with the control parameter, in order to identify the onset of secondary shearless tori, i.e. shearless tori that appear within the islands of stability [21]. It is noteworthy that both twist and nontwist maps used in [21] are symmetric maps, which implies a variety of symmetry lines spread all over the phase space. Furthermore, the calculus of the rotation number in [21] was made on these symmetry lines. Owing to the toroidal geometry, most of the maps used to describe magnetic surfaces in tokamaks are not symmetric. Thus, it makes sense to investigate secondary shearless tori in such systems and also their consequences to the plasma confinement.

In this paper, we consider the perturbation created by an ergodic limiter in the equilibrium tokamak field to cause selective destruction of magnetic surfaces in this region, giving rise to chaotic layers and several resonant regular islands at the plasma edge [4–6]. We apply our numerical procedure to find secondary shearless bifurcations in the Ullmann map, a twist symplectic map introduced to describe chaotic field lines in tokamaks with an ergodic limiter [22]. We identify the onset of secondary shearless tori around elliptic fixed points within the island of stability by examining numerical profiles of the internal rotation number. Once the secondary shearless tori are identified in the system, we focus on studying their consequence on transport. We observe that the rupture of the secondary shearless tori near the chaotic edge leads to a sudden reduction in the escape of the magnetic field lines.

The paper is organized as follows. Section 2 presents the basic magnetic field line equations, the formulae that are used throughout the paper and examples of field line phase spaces. Section 3 introduces the procedure used to identify the secondary shearless bifurcations and contains examples of these bifurcations. Section 4 presents results on the stickiness, associated with the identified bifurcation, which reduces the field line transport. The conclusions are in section 5.

2. Magnetic field lines

The geometry of a tokamak is determined by its major (R_0) and minor (b) radii (see the scheme in figure 1). For large aspect ratio, i.e. $R_0/b \gg 1$, we can consider a cylindrical approximation in coordinates (r, θ, z), whose axis of symmetry z is related to the toroidal angle ϕ by $z = R_0\phi$. The magnetic field lines are determined by $\boldsymbol{B} \times \mathrm{d}l = 0$ which, in the cylindrical coordinates, can be written as

$$\frac{\mathrm{d}r}{B_r} = \frac{r\,\mathrm{d}\theta}{B_\theta} = \frac{R_0\,\mathrm{d}\phi}{B_\phi} = \frac{\mathrm{d}z}{B_\phi}. \tag{1}$$

The unperturbed field, $\boldsymbol{B}_0$, is a superposition of the toroidal field $B_\phi = B_z$, created by external coils and a poloidal field B_θ, due to the plasma current I_p, i.e. $\boldsymbol{B}_0(r) = (B^0_r = 0, B^0_\theta(r), B^0_\phi(r))$. Under previous assumptions, the toroidal field B_ϕ is, practically, uniform and the magnetic surfaces are considered to be circular and concentric (the toroidal correction will be introduced later on). On the other hand, magnetic perturbations of the form $\boldsymbol{B}_1(r, \theta, \phi) = (B^1_r(r, \theta, \phi), B^1_\theta(r, \theta, \phi), B^1_\phi = 0)$ are generated when one introduces external magnetic devices in the tokamak. In this paper, we will consider an ergodic magnetic limiter (EML).

The EML is a grid-shaped current ring poloidally wound around the tokamak. Its ring consists of a coil of width l, with m pairs of wires along the toroidal direction carrying a current I_h (see figure 1). Basically, the EML is a device designed to generate external magnetic fields that interact with the equilibrium tokamak field causing a destruction of boundary magnetic surfaces. In order to describe the effect of the EML on the magnetic surfaces, we will recall a symplectic map previously introduced in [20].

2.1. The Ullmann map

An appreciative tool to study the magnetic field lines is the Poincaré map. In the poloidal surface $z = cte$ (the said Poincaré surface), the Poincaré map relates the n_{th} intersection point, (r_n, θ_n), to the next one, (r_{n+1}, θ_{n+1}), after one toroidal turn. In this paper, we recall a symplectic map that describes the behaviour of magnetic field lines in the presence of an

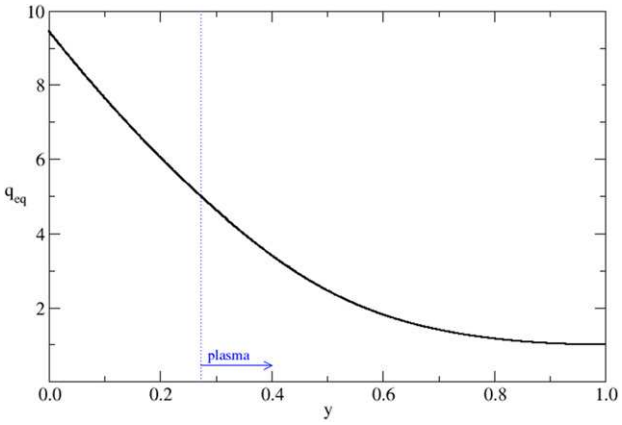

Figure 2. Monotonic safety factor profile given by equation (4) with $q_a = 5$ and $\gamma = 4$. The abscissa is in the rectangular normalized coordinates: $y = 1 - r/b$.

ergodic limiter. The mentioned map was obtained in [20] and it is constituted by the convolution of two maps, $\hat{\boldsymbol{F}} = F_1 \circ F_2$. The first one is the equilibrium map:

$$F_1 : \begin{cases} r_{n+1} = \dfrac{r_n}{1 - a_1 \sin\theta}, \\ \theta_{n+1} = \theta_n + \dfrac{2\pi}{q_{\rm eq}(r_{n+1})} + a_1 \cos\theta_n, \end{cases} \tag{2}$$

where a_1 is a correction for toroidal effect giving rise to a difference between the geometric axis and the magnetic axis (*Shafranov shift*). The function $q_{\rm eq}$ is the equilibrium safety factor defined by

$$q_{\rm eq}(r) = \left\langle \frac{{\rm d}\phi}{{\rm d}\theta} \right\rangle = \frac{1}{2\pi} \int_0^{2\pi} \left(\frac{{\rm d}\phi}{{\rm d}\theta} \right) {\rm d}\theta, \tag{3}$$

where from equation (1), ${\rm d}\phi/{\rm d}\theta = rB_\phi/R_0 B_\theta$. Following [23], we consider the safety factor

$$q_{\rm eq}(r) = \begin{cases} q_a \dfrac{r^2}{a^2} \left\{ 1 - \left(1 - \dfrac{r^2}{a^2} \right)^{\gamma+1} \right\}^{-1} & (0 \leqslant r \leqslant a), \\ q_a \dfrac{r^2}{a^2} & (a \leqslant r \leqslant b), \end{cases} \tag{4}$$

which is a monotonic function toned by the parameters γ and q_a to fit plasma discharges observed in typical tokamak experiments. We show in figure 2 the profile described by equation (4) with $q_a = 5$ and $\gamma = 4$. Note that the safety factor goes to 1 in the plasma core, while higher values are concentrated near the tokamak wall ($y = 0$, see the rectangular transformation in section 2.2).

The perturbation map emerges from the effect of the ergodic limiter on the equilibrium configuration and it is defined by

$$F_2 : \begin{cases} r_{n+1} = r^*_{n+1} + \dfrac{mC\epsilon b}{m-1} \left(\dfrac{r^*_{n+1}}{b} \right)^{m-1} \sin(m\theta_{n+1}), \\ \theta^*_{n+1} = \theta_{n+1} - C\epsilon \left(\dfrac{r_{n+1}}{b} \right)^{m-2} \cos(m\theta_{n+1}), \end{cases} \tag{5}$$

with $C = 2mla^2/R_0 q_a b^2$ and ϵ being the perturbation parameter related to the ratio between the limiter and plasma currents, $\epsilon = I_h/I_{\rm p}$. We should note that r^*_{n+1} in equation (5) is not separable, thus, a numerical method for finding roots (such as the Newton–Raphson method) is required. Nevertheless, the map $\hat{\boldsymbol{F}}$ is strictly area-preserving and can describe field line behaviour in tokamaks with ergodic limiters in a practical way, since we do not have to numerically integrate the field line equations over the toroidal revolution. The advantages of the Ullmann map over previous maps, used to describe magnetic surfaces perturbed by resonances, are the use of parameters more closely related to measurable physical quantities (such as the safety factor and limiter current) and the consideration of toroidal effects. In addition, the Ullmann map satisfies the conditions for a tokamak model outlined in [24].

2.2. Typical phase spaces

As commented previously, a point in the tokamak is determined by its cylindrical coordinates (r, θ, z) with respect to the symmetry axis. Since the EML aims to modify the magnetic surfaces close to the tokamak wall, it is common to replace the cylindrical coordinates by rectangular ones: $x = b\theta$ and $y = b - r$ [25]. Hence, the tokamak wall is characterized by the line segment $y = 0$, with $x \in [0; 2\pi b]$. In the following phase spaces, we will use the normalized coordinates $x = x/b$ and $y = y/b$. In this paper, we choose a set of parameters typical for large aspect ratio small tokamaks: $a_1 = -0.04$, $R_0 = 0.3\,{\rm m}$, $b = 0.11\,{\rm m}$, $a = 0.08\,{\rm m}$ and $l = 0.08\,{\rm m}$.

In the unperturbed case ($\epsilon = 0$), the dynamic of the Ullmann map is dictated by the equilibrium map (equation (2)). Thus, the trajectories lie on invariant lines in the phase space when the rotation number, Ω, is irrational (invariant tori). Otherwise, rational rotation numbers, $\Omega = n/m$ (n, m integer), are related to periodic points in the phase space. In figure 3(*a*) we observe the unperturbed phase space of the Ullmann map mostly filled by invariant tori.

For $\epsilon \neq 0$, some invariant curves are destroyed forming a thin chaotic layer near resonant islands. In the Ullmann map, the perturbation parameter affects, primarily, the m-mode resonances, i.e. chaotic trajectories will be produced in the vicinity of resonances of periodicity m, where m is a parameter related to the number of pairs of straight wires of the EML. Therefore, in order to introduce chaotic trajectories near the tokamak wall ($y = 0$), we should choose integer values of m given by the safety factors near the tokamak wall. In our case, it is enough to consider $m > 5$ (see in figure 2 that safety factors higher than 5 are out of the plasma region). In figure 3(*b*) we see the phase space for $\epsilon = 0.05$ and $m = 6$. In this case, we note that the perturbation parameter is enough to destroy some magnetic surfaces near the tokamak wall giving rise to period-6, -7 and -8 island chains, respectively, as we can easily observe in the phase space of figure 3(*b*).

3. Secondary shearless magnetic surfaces

3.1. The global shearless structure

Generally, the safety factor represents the shear of helical magnetic fields. Therefore, in terms of the two-dimensional phase space, the rotation $\Omega(r)$ of the magnetic surfaces is

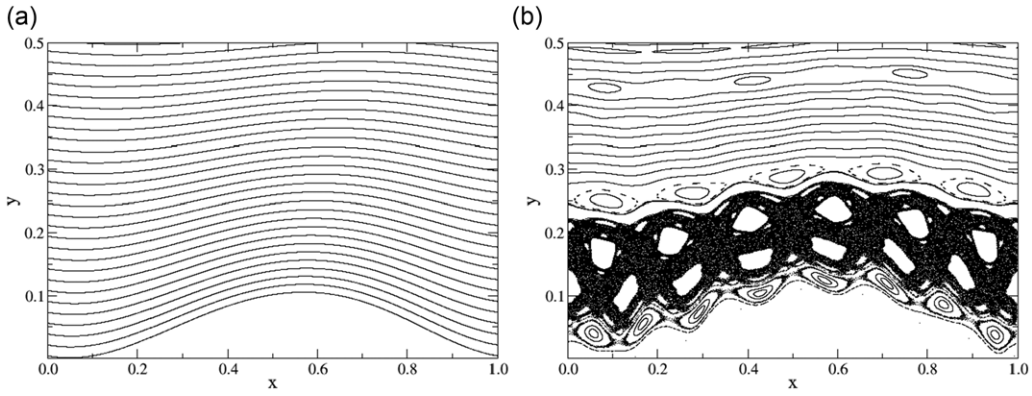

Figure 3. Phase spaces of the Ullmann map with $m = 6$ and (a) $\epsilon = 0$; (b) $\epsilon = 0.05$.

defined as the average poloidal angle of displacement of a given field line in the course of a complete toroidal turn around the tokamak. Thus,

$$\Omega(r) \sim \left\langle \frac{\mathrm{d}\theta}{\mathrm{d}\phi} \right\rangle \sim \frac{1}{q(r)}. \tag{6}$$

Now, let us consider that $\Omega(r)$ does not satisfy the nondegeneracy condition, also called the twist condition:

$$\frac{\mathrm{d}\Omega(r)}{\mathrm{d}r} \neq 0. \tag{7}$$

So, it means that $\Omega(r)$ is a nonmonotonic function and there is at least one value $r = r_c$ for which the shear of the rotation vanishes, $\mathrm{d}\Omega(r)/\mathrm{d}r = 0$ at $r = r_c$. If a system does not satisfy the twist condition (equation (7)), it is called nontwist and the point r_c is a shearless point. In the phase space, r_c defines a shearless torus whose main feature is the resistance to perturbation, implying a barrier to the transport [18]. In addition, nontwist systems exhibit nontrivial bifurcations due to separatrix reconnection [19], which are not observed in typical twist systems.

In the context of magnetically confined plasmas it is natural to expect that robust magnetic surfaces (shearless) are possible only for reversed shear magnetic field configurations. Nevertheless, we will show that although a monotonic safety factor for the Ullmann map (equation (4)) does not imply a global shearless magnetic surface, it may appear, secondarily, in resonant islands close to some bifurcations.

3.2. Secondary shearless tori

Recently, the presence of one shearless torus was analytically predicted for a generic Hamiltonian system in the neighbourhood of the tripling bifurcation of an elliptic fixed point [20]. Furthermore, numerical investigations [21] suggest a specific profile containing two shearless tori near the quadrupling (1/4) bifurcation.

As we are interested in localized regular islands immersed in chaotic regions of the phase space of our model, it becomes important to study the emergency of these secondary shearless tori. Hence, we use the internal rotation number to measure the torsion of each torus with respect to its elliptic fixed point.

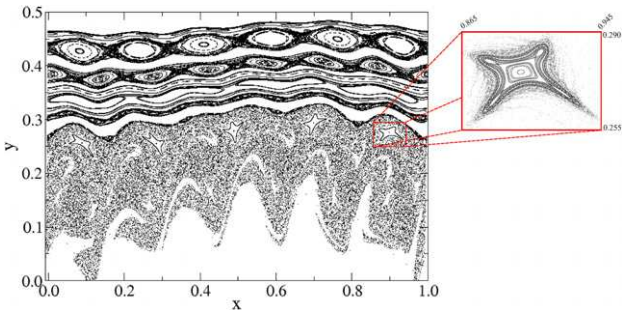

Figure 4. Phase space of the Ullmann map with $\epsilon = 0.189$ and $m = 6$. The red box emphasizes the quadrupling bifurcation.

It is defined as

$$\omega_{\mathrm{in}} = \lim_{n\to\infty} \frac{1}{2\pi n} \sum_{n=1}^{\infty} P_n(x, y)\hat{\theta} P_{n+1}(x, y), \tag{8}$$

where $P_n\hat{\theta}P_{n+1}$ means the angle θ between two consecutive points and (x, y) are the coordinates of the two-dimensional map. The angle θ is normalized by 2π so that the values returned belong to the range [0,1]. By equation (8) a rational internal rotation number (n/m) describes a periodic orbit while an irrational number represents a circular quasi-periodic orbit. For a chaotic orbit, equation (8) does not converge.

Owing to the numerous resonant island chains in the Ullmann map, the tripling or quadrupling bifurcation of a elliptic fixed point may appear in the phase space over a large range of ϵ. To illustrate the emergency of the secondary shearless torus within the islands of stability, we choose a value for ϵ that presents a phase space whose chaotic layer near the border $y = 0$ is composed of only one visible remaining island chain. See in figure 4 the period-5 island chain whose elliptic fixed point has bifurcated in a period-4 one (amplification red box).

The evolution of the internal rotation number profiles to the highlighted island in figure 4 is shown in figure 5. The internal rotation number is calculated following equation (8) with initial conditions lying in the straight line indicated in figure 5(a) (dashed line). For $\epsilon = 0.185$ (figure 5(a)) the internal rotation number profile is monotonic, i.e. each specific value of ω_{in} is related to only one circular invariant torus. Increasing the parameter to $\epsilon = 0.187$ is sufficient for the

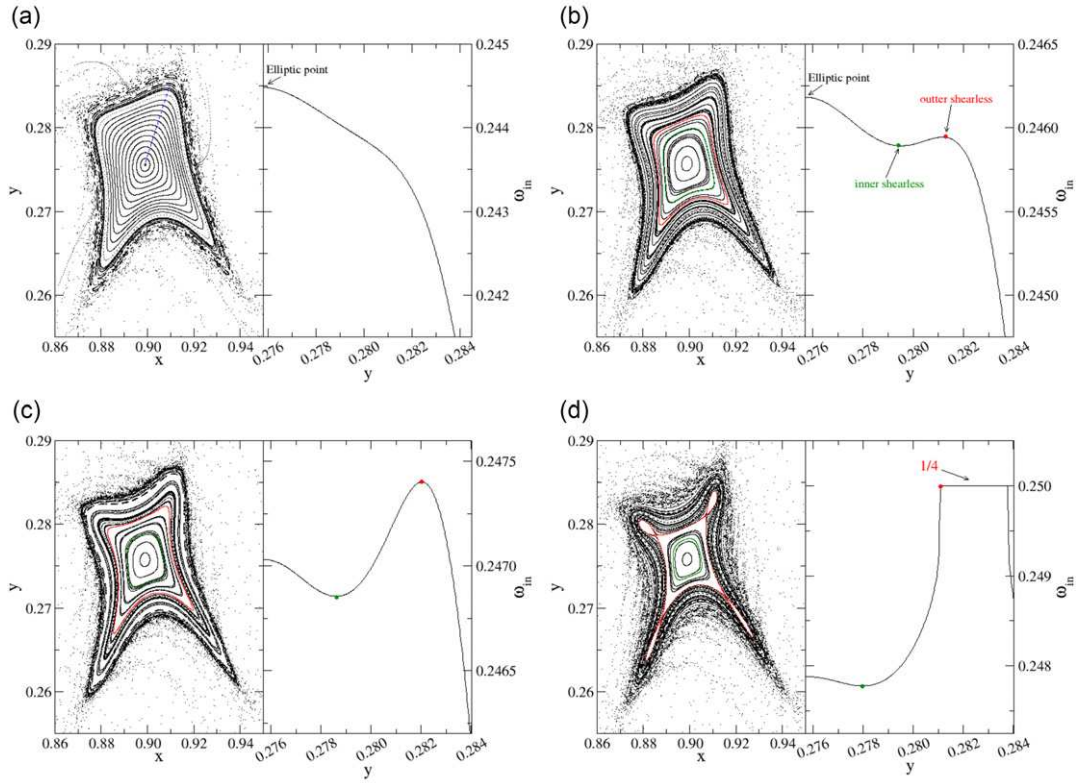

Figure 5. The quadrupling bifurcation in the Ullmann map. (*a*) $\epsilon = 0.185$; (*b*) $\epsilon = 0.187$; (*c*) $\epsilon = 0.188$ and (*d*) $\epsilon = 0.189$. Note that the onset of two s-shearless tori arose for some value of ϵ between (*a*) and (*b*).

formation of bumps, as shown in figure 5(*b*). The presence of a minimum and a maximum point in the rotation profile indicates the existence of two tori without shear. Consequently, the same rotation number may repeat up to three times.

Figure 5(*c*) emphasizes the growth of bumps as we increase the perturbation parameter to $\epsilon = 0.188$. For $\epsilon = 0.189$, figure 5(*d*), the maximum bump reaches the value $\omega_{in} = 1/4$ yielding four stable fixed points, so long as the minimum bump still exists and does not bifurcate for any lower order rational number and ends colliding with the elliptic fixed point. The scenario described previously matches with the results presented in [21] for period-4 bifurcation in the standard map.

In spite of the fact that secondary shearless tori are local phenomena and, consequently, do not interfere in the global properties of the chaotic layer, it is relevant, in the tokamak context, to study the transport process while these secondary shearless tori exist.

4. Transport

In order to investigate the dependence of the transport properties on the initial conditions and the perturbation parameter ϵ, chosen near the values for period-4 bifurcation, we computed the average escape time of orbits by the following numerical experiment. For a given value of ϵ, we tested a large number of initial points ($N_P = 2 \times 10^6$) placed on a regularly spaced grid of the same size as in figure 5. Each initial condition was iterated until the corresponding orbit crossed the reference boundary $y = 0$. The average escape time is shown in figure 6. From figure 6 we observe a strong dependence on ϵ with several peaks in the escape time close to bifurcations. The higher peak, $\epsilon = 0.189\,95$, corresponds to the lower order bifurcation ($\frac{1}{4}$) observed in the range $\epsilon \in [0.180 : 0.200]$ and represents the limit to the existence of the secondary shearless torus shown in figure 5. This atypical escape time around a specific value of ϵ indicates some kind of trapping mechanism that hinders the transport. To illustrate the transport for different choices of ϵ we show in figure 7 fine details of the dependence of the escape time on the initial conditions, for two values of ϵ: one of them corresponds to short escape time (blue dotted line labelled (a) in figure 6) and the second to long escape time (red dashed line labelled (*b*) in figure 6). Each initial condition was iterated 3×10^6 times and the different escape times are indicated by a logarithmic colour scale. From figure 7 we see that points inside the islands, evidently, do not escape and are identified with red colour, but the orbits adjacent to them may spend long or short time to reach the reference boundary $y = 0$. By comparing figures 7(*a*) and (*b*) it becomes clear that both are composed, mainly, of short and medium escape times. Nevertheless, figure 7(*b*) presents a reasonable amount of initial conditions that spend long times ($\approx 1 \times 10^6$, orange colour) encircling the island. Such a phenomenon is called stickiness and indicates a long-term stay of the trajectories in the region performing an almost regular motion. The type of stickiness interferes in the average escape time and, consequently, in the global transport of the system (see more about stickiness and transport in [14, 26] and references therein).

A statistical distribution of the escape time in the phase space can be used to characterize such a stickiness process.

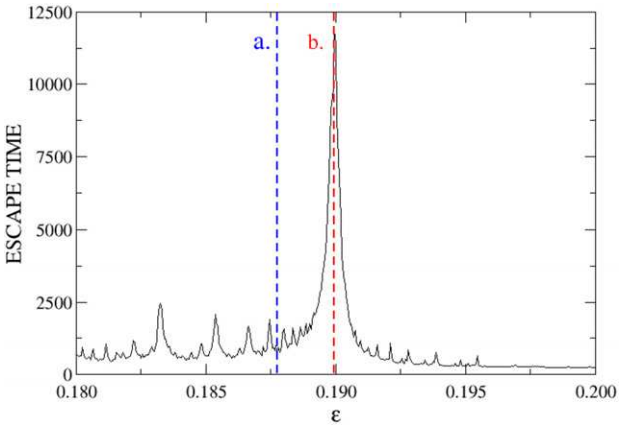

Figure 6. Escape time calculated for a grid of initial conditions in the localized phase space studied in figure 5.

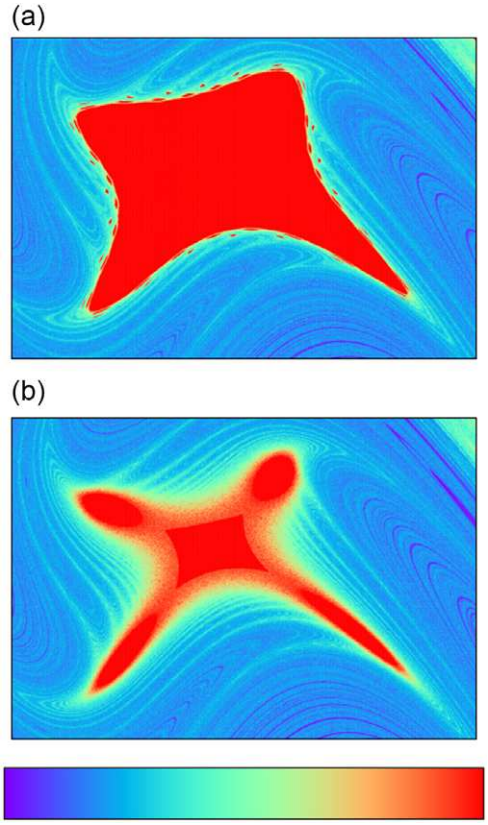

Figure 7. Escape time for initial conditions in the chaotic layer of the Ullmann map with (*a*) $\epsilon_a = 0.187\,75$ and (*b*) $\epsilon_b = 0.189\,95$. The colour scale represents short (1 iteration, dark blue) to long escape times (3×10^6 iterations, red).

Thus, we computed the escape time statistic (ETS) for a large number of chaotic initial conditions placed near the reference boundary $y = 0$ and far from the island chain. We choose this region for the initial conditions in order to understand whether the island chain is able to capture trajectories initiated far from it. The ETS is defined as

$$\rho(\tau) = \frac{M_n}{M}, \tag{9}$$

where M_n is the number of initial conditions that crossed the boundary $y = 0$ with iteration numbers (time) $n \geqslant \tau$ and M is the total number of initial conditions that actually crossed the boundary. In fact, equation (9) is a cumulative distribution function that decreases from $\rho(0) = 1$. Figure 8 shows the ETS for both cases $\epsilon_a = 0.187\,75$ and $\epsilon_b = 0.189\,95$.

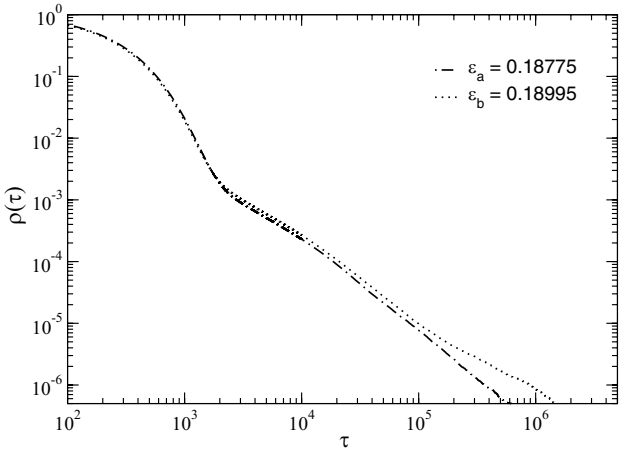

Figure 8. ETS for a large number of initial conditions with $\epsilon_a = 0.187\,75$ and $\epsilon_b = 0.189\,95$.

For times $\tau < 10^3$, the ETS for $\epsilon_a = 0.187\,75$ and $\epsilon_b = 0.189\,95$ has the same exponential decay. As the exponential decay is related to the randomness of the chaotic layer we can, initially, conclude that the chaotic extension of both cases is quite similar. Nonetheless, for $\tau > 10^3$ the ETS decays as a power law, which indicates the presence of some kind of trapping in the phase space. During $10^3 < \tau < 10^5$ the ETS for $\epsilon_a = 0.187\,75$ and $\epsilon_b = 0.189\,95$ presents the same decay although the values are different. However, for long times, $\tau > 10^5$, the ETS indicates different behaviour between both cases and according to figure 8 the island chain that remains during the perturbation, $\epsilon_b = 0.189\,95$, captures a larger amount of initial conditions, which spend long times encircling it, than the case $\epsilon_a = 0.187\,75$, which explains the modification in the tail of the ETS.

5. Conclusion

We addressed the chaotic transport of magnetic field lines in a tokamak plasma edge. In our work, the resonant perturbations that break the magnetic surfaces are those created by an external ergodic limiter. In this case, the perturbed field line mapping is approximately obtained, for large aspect ratio tokamaks, from the symplectic Ullmann map [20]. The Ullmann map allows us to analyse the influence of the relevant control parameters, related to the equilibrium and perturbing fields, on the transport of field lines. More specifically, we use the obtained map to investigate the onset of secondary shearless curves in equilibria with monotonic safety factor profiles and how this bifurcation affects the plasma edge transport. The results reported in this work due to external resonant perturbations are also expected to be valid for spontaneous resonant fluctuations commonly observed in the confined plasma.

For a monotonic plasma current (or safety factor) profile, i.e. for a twist mapping of field lines, we present examples of secondary shearless invariant onset followed by bifurcations

that create new secondary islands with high stickiness around them. This stickiness that appears with the new islands reduces the field line escaping to the wall. Thus, from our results, we observe that whenever the secondary shearless curves appear they may be followed by a reduction in transport if the control parameter, the magnetic shear or the perturbation amplitude, is properly altered. We would like to remember that tripling and quadrupling bifurcations creating, respectively, three and four islands, have been reported after the onset of secondary shearless invariants [21]. Complementarily, other examples of stickiness enhancement in symplectic maps due to triple bifurcations, similar to those reported in this paper, have been recently reported [27]. We should note that the stickiness enhancement is not a phenomenon directly related to the secondary shearless tori but it is a consequence of their existence. Our results indicate that although higher order bifurcations may also be found they should be less common. Finally, we conjecture that an alteration of the amplitude of spontaneous or external resonant perturbations may create shearless curves and associated bifurcations significantly reducing the particle transport at the plasma edge.

Acknowledgments

The authors thank Brazilian scientific agencies: CAPES, CNPq and São Paulo Research Foundation (FAPESP) for financial support through grants 2010/00740-6 and 2011/19269-11.

References

[1] Boozer A.H. 2005 *Rev. Mod. Phys.* **76** 1071
[2] Jakubowski M.W., Schmitz O. and Abdullaev S.S. 2006 *Phys. Rev. Lett.* **96** 0350041
[3] Evans T.E. *et al* 2005 *Nucl. Mater.* **337–339** 691
[4] Mccool S.C. *et al* 1989 *Nucl. Fusion* **29** 547
[5] Karger F. and Lackner K. 1977 *Phys. Lett.* A **61** 385
[6] Caldas I.L. *et al* 2002 *Braz. J. Phys.* **32** 980
[7] Gendrich Ph, Grosman A. and Caps H. 1996 *Plasma Phys. Control. Fusion* **38** 1653–724
[8] Jakubowski M.W., Abdullaev S.S. and Finken K.H. 2004 *Nucl. Fusion* **44** S1
[9] Caldas I.L. *et al* 2012 *Plasma Phys. Control. Fusion* **54** 124035
[10] Levinton F.M. *et al* 1995 *Phys. Rev. Lett.* **75** 4417
[11] Strait E.J. *et al* 1995 *Phys. Rev. Lett.* **75** 4421
[12] Lichtenberg N. and Lieberman M.A. 1992 *Regular and Chaotic Dynamics* 2nd edn (Berlin: Springer)
[13] Morrison P.J. 2000 *Phys. Plasmas* **7** 2279
[14] Meiss J.D. 1992 *Rev. Mod. Phys.* **64** 795
[15] Abdullaev S.S. *et al* 1998 *Phys. Plasmas* **5** 196
[16] Egydio de Carvalho R. and Ozorio de Almeida A. M. 1992 *Phys. Lett.* A **162** 457
[17] Howard J.E and Hohs S.M. 1984 *Phys. Rev.* A **29** 418
[18] Del-Castillo-Negrete D., Greene J.M. and Morrison P.J. 1996 *Physica* D **91** 1
[19] Wurm A. *et al* 2005 *Chaos* **15** 023108
[20] Dullin H.R., Meiss J.D. and Sterling D. 2000 *Nonlinearity* **13** 203
[21] Abud C.V. and Caldas I.L. 2012 *Chaos* **22** 033142
[22] Ullmann K. and Caldas I.L. 2000 *Chaos Solitons Fractals* **11** 2129
[23] Caldas I.L. *et al* 1996 *Chaos Solitons Fractals* **7** 991
[24] Balescu R., Vlad M. and Spineanu F. 1998 *Phys. Rev.* E **58** 951
[25] Martin T.J. and Taylor J.B. 1984 *Plasma Phys. Control. Fusion* **26** 340
[26] Zaslavsky G.M. 2002 *Phys. Rep.* **371** 461
[27] Szezech J.D. *et al* 2009 *Chaos* **19** 043108